Assessing pyroclastic fall hazard through field data and numerical simulations: Example from Vesuvius

Raffaello Cioni,[1] Antonella Longo,[2] Giovanni Macedonio,[3] Roberto Santacroce,[2] Alessandro Sbrana,[2] Roberto Sulpizio,[2] and Daniele Andronico[4]

Received 12 April 2001; revised 2 April 2002; accepted 7 May 2002; published 1 Feburary 2003.

[1] A general methodology of pyroclastic fall hazard assessment is proposed on the basis of integrated results of field studies and numerical simulations. These approaches result in two different methods of assessing hazard: (1) the ''field frequency,'' based on the thickness and distribution of past deposits and (2) the ''simulated probability,'' based on the numerical modeling of tephra transport and fallout. The proposed methodology mostly applies to volcanoes that, by showing a clear correlation between the repose time and the magnitude of the following eruptions, allows the definition of a reference ''maximum expected event'' (MEE). The application to Vesuvius is shown in detail. Using the field frequency method, stratigraphic data of 24 explosive events in the 3–6 volcanic explosivity index range in the last 18,000 years of activity are extrapolated to a regular grid in order to obtain the frequency of exceedance in the past of a certain threshold value of mass loading (100, 200, 300, and 400 kg/m^2). Using the simulated probability method, the mass loading related to the MEE is calculated based on the expected erupted mass (5×10^{11} kg), the wind velocity profiles recorded during 14 years, and various column heights and grain-size populations. The role of these factors was parametrically studied performing ~160,000 simulations, and the probability that mass loading exceeded the chosen threshold at each node was evaluated. As a general rule, the field frequency method results are more reliable in proximal regions, provided that an accurate database of field measurements is available. On the other hand, the simulated probability method better describes events in middle distal areas, provided that the MEE magnitude can be reliably assumed. In the Vesuvius case, the integration of the two methods results in a new fallout hazard map, here presented for a mass loading value of 200 kg/m^2. *INDEX TERMS:* 8404 Volcanology: Ash deposits; 3210 Mathematical Geophysics: Modeling; 1035 Geochemistry: Geochronology; 5480 Planetology: Solid Surface Planets: Volcanism (8450); 9335 Information Related to Geographic Region: Europe; *KEYWORDS:* Vesuvius, ash fallout, explosive eruptions, volcanic hazard, numerical modeling, hazard mapping

Citation: Cioni, R., A. Longo, G. Macedonio, R. Santacroce, A. Sbrana, R. Sulpizio, and D. Andronico, Assessing pyroclastic fall hazard through field data and numerical simulations: Example from Vesuvius, *J. Geophys. Res.*, *108*(B2), 2063, doi:10.1029/2001JB000642, 2003.

1. Introduction: Criteria for Hazard Assessment

[2] Volcanic activity shows a great variability of eruptive processes that are potentially hazardous (tephra fallout, pyroclastic flow, lava invasion, gas emission, debris avalanche, structural collapse, lahar, etc.), in some cases characterized by a time-dependent, gradual impact on the territory (e.g., the lava front motion, the static pressure of tephra blankets, the concentration of toxic gases). When assessing the volcanic hazard of an area each particular type of volcanic process (expected to be potentially hazardous) needs to be defined using some specific threshold values, which qualify its peculiar ability to have a dangerous impact on the territory and/or on population. The volcanic hazard of a given area within a given time interval is therefore the product of several partial hazards, each resulting from three different probabilities concerning: (1) the occurrence of the eruption, (2) the occurrence of the considered phenomenon, and (3) the exceeding of the chosen threshold in the chosen area.

[3] The nearly constant eruptive behavior of many frequently erupting volcanoes, which are generally characterized by open conduit conditions (e.g., Kilauea, Sakurajima, Piton de la Fournaise, Etna), allows a reliable estimate of their eruption frequency as well as of the main associated hazardous phenomena. Otherwise, when dealing with dormant volcanoes, the accuracy in the assessment of timing of their

[1]Dipartimento di Scienze della Terra, Università degli Studi di Cagliari, Cagliari, Italy.
[2]Dipartimento di Scienze della Terra, Università degli Studi di Pisa, Pisa, Italy.
[3]Istituto Nazionale di Geofisica e Vulcanologia-Osservatorio Vesuviano, Naples, Italy.
[4]Istituto Nazionale di Geofisica e Vulcanologia-Catania, Nicolosi Catania, Italy.

0148-0227/03/2001JB000642$09.00

reactivation is quite hard to evaluate, as well as the size of the future eruption and the associated sequence of phenomena. In these cases the hazard can be assessed under the assumption of the future occurrence of a predetermined event (e.g., the largest, the most frequent, the most hazardous), to be chosen on the basis of the eruptive history of the volcano.

[4] At volcanoes whose activities have shown recurrent or clearly defined patterns, a useful concept is that of the maximum expected event (MEE), defined as the largest out of all the possible eruptions within a certain time window [*Barberi et al.*, 1990]. The MEE represents also the reference event on which numerical simulations aimed at hazard assessment has to be based. The selection of the MEE involves the assumption of an expected eruption scenario that accounts, by analogy with historical and volcanological data, on past eruptions, for the most likely association and sequence of eruptive, possibly hazardous, phenomena. Thus, having fixed the eruption and the expected scenario, hazard assessment requires defining the probability that an area will be affected by the selected hazardous phenomenon.

[5] In this paper, results of tephra fallout hazard assessment at Vesuvius, based on field studies and numerical simulations of MEE, are matched. The two approaches result in two different types of output data: ''field frequency'' of the past fallout deposits and ''simulated probability'' of the fallout deposits obtained by numerical simulations of MEE. Their integration represents a significant improvement in hazard zonation at Vesuvius and provides a general methodology, which can be applied to other areas and to different phenomena.

[6] In order to avoid misunderstandings or misinterpretations in the terminology used in the following, some main definitions are worth presenting hazard, the probability that a given event will induce an undesired effect; threshold value, a value of a physical variable (thickness, velocity, mass loading, etc.) that might be exceeded to induce the undesired effect; field frequency, the fraction of past events (eruptions) which exceeded the threshold value; MEE, the largest out of all the possible eruptions to be expected in a given time window; and simulated probability, the percentage of events exceeding the threshold in a numerically simulated set of events.

2. Vesuvius Case

[7] Since its last eruption, in March 1944, Vesuvius has remained dormant and no actual ''signs'' suggest impending unrest. However, during its eruptive history Vesuvius often experienced long periods of quiescence that lasted, in some cases, centuries or tens of centuries, with an ''awakening'' more and more violent the longer the repose-time preceding the eruption. Vesuvius has a relatively brief eruptive history. The Somma stratovolcano, the oldest edifice, formed mainly by lavas in a short time between 37 and 20 ka [*Andronico et al.*, 1995]. The volcano experienced an abrupt change in the style of activity around 18 ka (Figure 1), when the first and largest Plinian event (Pomici di Base eruption [*Bertagnini et al.*, 1998]) occurred. Related to this eruption, a polyphased caldera began to form, continuously changing and enlarging after each major explosive event [*Cioni et al.*, 1999]. Other Plinian eruptions occurred at 8 ka (Pomici di Mercato), 3.8 ka (Pomici di Avellino), and on A.D. 79

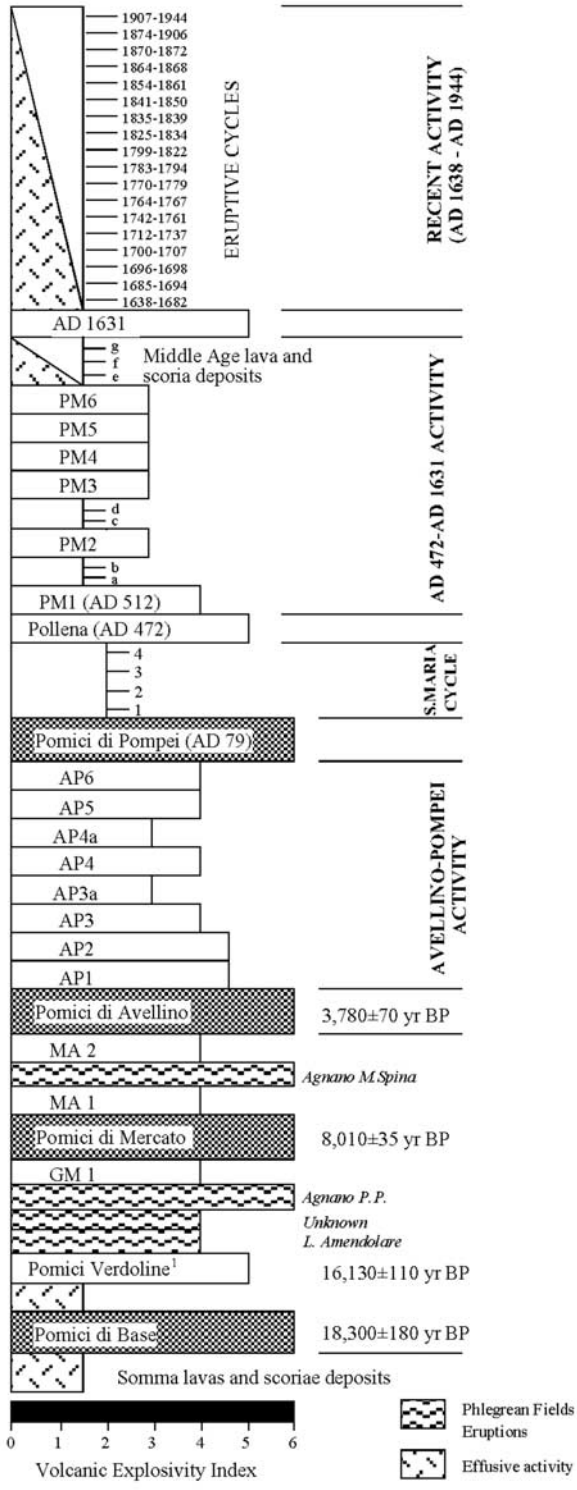

Figure 1. Chronostratigraphy of Vesuvius in the last 18 kyr. Radiocarbon ages from *Andronico et al.* [1995]. Also called Greenish Eruption [*Santacroce*, 1987].

(''Pompeii'' eruption). Several sub-Plinian outbursts punctuated the inter-Plinian periods, the two most recent occurring in A.D. 472 and A.D. 1631. Alternating with these major eruptions, several smaller explosive eruptions occurred. Evidences of lava effusions and cone building phases are lacking between about 15 ka and the A.D. 79

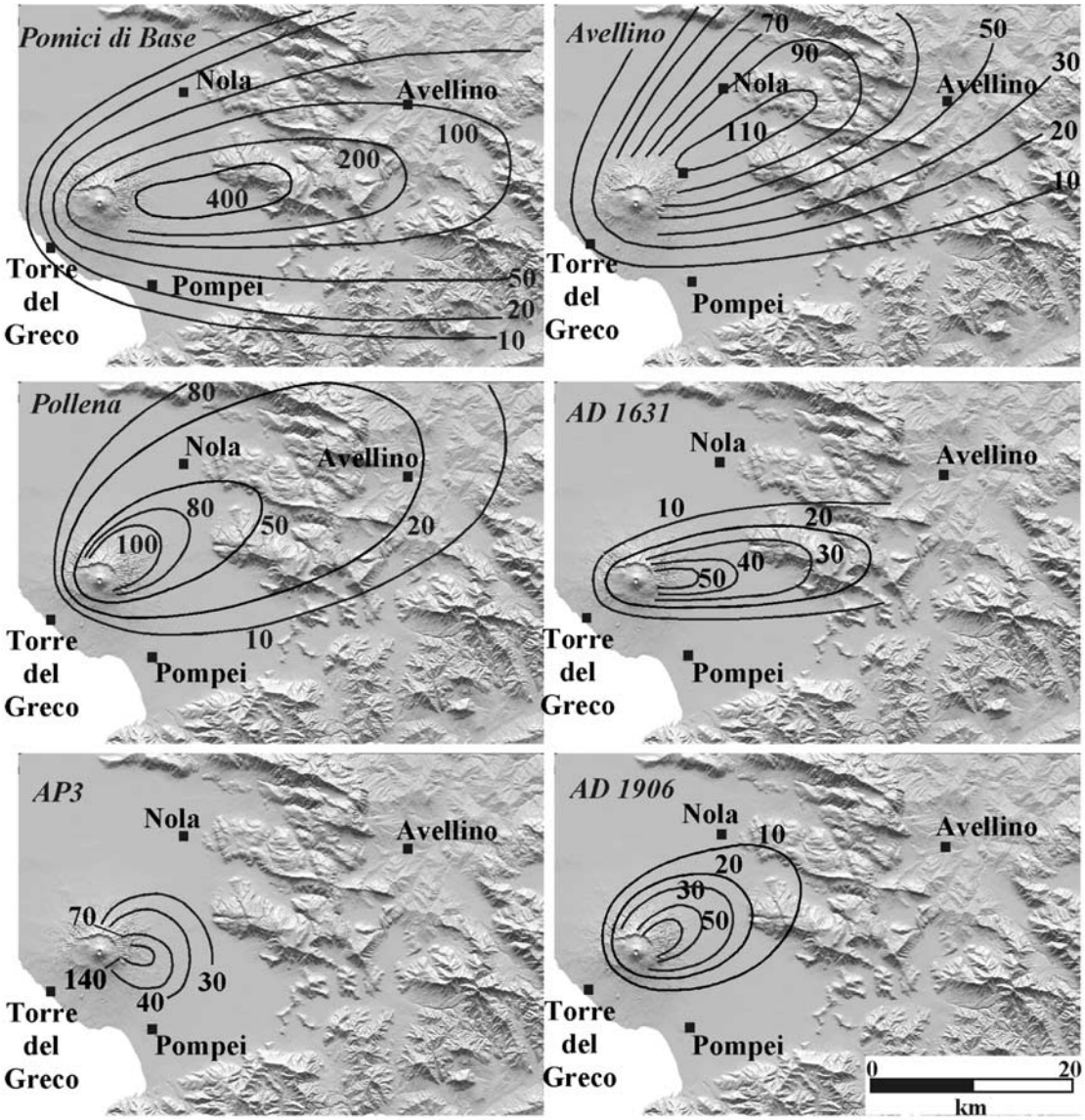

Figure 2. Isopach maps of selected eruptions at Vesuvius. For each class of event, the deposit corresponding to two extremes of magnitude are shown: VEI-6 Plinian (''Pomici di Base'' and ''Avellino''), VEI-5 sub-Plinian (''Pollena'' and ''A.D. 1631''), and VEI-3/VEI-4 Vulcanian to violent Strombolian (''AP3'' and ''1906''). Thickness is expressed in cm.

eruption. All the explosive eruptions were characterized by a paroxysmal fallout phase, which deposited tephra blankets around the volcano over thousands of km^2. An important increase in the eruption frequency followed the ''Pomici di Avellino'' Plinian eruption, and was marked by a progressively larger number of events per unit time accompanied by decreasing erupted volume associated with each event.

[8] The pyroclastic fall deposits of the larger eruptions typically consist of highly vesicular pumice, resulting in a low bulk density of the deposit. Wet, dense, phreatomagmatic ash is very frequent in the fallout sequences of many eruptions, increasing the mass loading due to their higher bulk density.

[9] When assessing fallout hazard in the Vesuvius area, a complication is represented by the presence of the Phlegrean Fields, a large caldera located about 25 km west of the volcano. In the last 18 ka, at least three pumice fallout blankets (Lagno Amendolare, Agnano Pomici Principali, and Agnano Monte Spina Plinian eruptions [*Andronico*, 1997; *Di Girolamo et al.*, 1984; *de Vita et al.*, 1999]) and some ash layers (e.g., Neapolitan Yellow Tuff [*Orsi et al.*, 1992]) reached Vesuvius and the area north of the volcano, increasing the frequency of tephra fallout in this sector. The circum-Vesuvian areas have been therefore frequently exposed to tephra deposition in the last 18,000 years. In this paper, hazard evaluation is restricted to Vesuvius activity, focusing on the probability of roof collapse related to mass loading from pyroclastics erupted as fallout products.

3. Maximum Expected Event (MEE) at Vesuvius

[10] Several authors have recently suggested that, despite the occurrence of some major eruptions which significantly affected the shallow magma system in the last 2000–3000

years, no major variations occurred in the composition of the feeding magma and in the mean deep magma supply rate at Vesuvius [*Santacroce et al.*, 1993; *Cioni et al.*, 1995, 1998]. Indeed, during this period, Vesuvius can be considered as a sort of steady state volcano, fed by the periodic arrival of high-T (1150–1200°C) K-tephritic magma batches [*Marianelli et al.*, 1995; *Cioni et al.*, 1995]. *Cortini and Scandone* [1982], on the basis of the A.D. 1754–1944 activity, estimated an average eruption rate of 1.6×10^6 m^3/yr. This value was used by *Barberi et al.* [1990] to assess a maximum eruptible mass of 2×10^{11} kg in the case of a short-term (20–30 years) reactivation of volcanic activity at Vesuvius. More recent papers [*Civetta and Santacroce*, 1992; *Santacroce et al.*, 1994] proposed a feeding rate 2–3 times larger. A major consequence is that the magma stored in the hypothesized reservoir growing under the volcano and available for the MEE has to be increased. A value of 5×10^{11} kg (2×10^8 m^3) is used in this paper. Such volume of magma, if totally ejected during a single explosive event, should be comparable to those emitted during A.D. 472 and A.D. 1631 eruptions [*Rosi and Santacroce*, 1983; *Rosi et al.*, 1993; *Rolandi et al.*, 1993], and belongs to the sub-Plinian range of magnitude of Vesuvius eruptions [*Arrighi et al.*, 2001]. During these events, fallout deposits were generally formed during the main phases of sustained convective column. On the contrary, coignimbritic ash deposits were very limited, due to the relatively small size of the pyroclastic density currents generated during these eruptions. In the last years, the A.D. 1631 eruption, for which reliable eyewitness accounts and recent volcanological studies exist [*Rosi et al.*, 1993; *Rolandi et al.*, 1993], was taken as the reference event for the scenario of the "maximum expected event (MEE)" of Vesuvius. The National Emergency Plan of the Vesuvian area adopted in 1995 was established on the basis of such a scenario, which involves, together with minor pyroclastic flow generation, the formation of a sustained convective eruptive column with the consequent downwind fallout of lapilli and ash.

Table 1. Main Physical Characteristics of the 24 Events (VEI 3–6) Used for the Geological Assessment of Mass Loading[a]

Eruption	VEI	H, km	A, km^2	V, $\times 10^6$ m^3	ρ, kg/m^3
A.D. 1944	3	4	270	110	1200
A.D. 1906	3	13[b]	210	80	1100
A.D. 1631	5	19	300	210[c]	1000
PM6	3	-	35	10	900
PM5	3	-			
PM4	3	-	60	100	900
PM3	3	-			
PM2	3	10	65	40	900
PM1	4	14	210	90	900
Pollena	5	-	1000	420	900
A.D. 79–472[d]	3	-	150	150	900
Pompeii W	6	26	1540	1100	500
Pompeii G	6	32	3430	1800	1000
AP5	4	-	180	80	1500
AP4	4	-	280	120	1300
AP3	4	15	350	150	1500
AP2	4–5	20	400	170	1500
AP1	4–5	-	300	150	1500
Avellino W	5	23	585	320[e]	400
Avellino G	6	31	2420	1250[e]	800
Mercato	6	22	2150	1400[f]	600
Verdoline	5	20	885	430	1000
Pomici di Base	6	-	2920	4400[g]	900

[a] For the largest events (VEI 6), the bulk density of the deposits was measured both at proximal and distal sites and show similar values, which are reported as unique value in the table. H is column height (following *Carey and Sparks* [1986]); A is area enclosed by the 10 cm isopach; V is total volume of the fall deposit (following *Pyle* [1989]); ρ is density of the fall deposit.
[b] *Arrighi et al.* [2001].
[c] *Rosi et al.* [1993].
[d] Total of four events.
[e] *Cioni et al.* [2000].
[f] From proximal data.
[g] *Bertagnini et al.* [1998].

4. Methods for Fallout Hazard Assessment

4.1. Fallout Hazard Assessment Using Field Data: Field Frequency Method

[11] The relative high frequency of fallout phenomena at Vesuvius and the well-preserved stratigraphic record allow the use of field data to assess the related hazard. Field data can be used to obtain hazard maps for fallout deposition based on thickness and weight per unit surface (mass loading) of tephra. Mass loading of tephra deposits is crucial in defining the level of possible damage to inhabited areas [*Blong*, 1984]. Since the critical mass loading expected for roof collapses largely varies depending on roof typology, reference values of 100, 200, 300, and 400 kg/m^2 were considered in this paper. These values correspond, in the circum-Vesuvian area, to about 5 to 40% of roof collapses [*Cherubini et al.*, 2001].

[12] In the following, the assessment of hazard was done based on field data from 24 out of about 30 significant explosive eruptions that occurred in the last 18 kyr. For all of them we were able to trace well-constrained dispersal maps (Figure 2), just based on scattered thickness measurements and their extrapolation to distal areas by means of the best fitting curve of exponential thickness decrease. On the basis of volume and dispersal of tephra fallout deposits, the volcanic explosivity index (VEI [*Newall and Self*, l982]) of these eruptions was evaluated between 3 and 6, corresponding to eruptions from violent Strombolian to Plinian (Table 1 and Figure 1). After visual tracing, the isopach maps were digitized and automatically extrapolated to a regular grid of 60 × 60 km around Vesuvius (500 m spacing), in order to derive thickness values at each node of the grid. The values were then transformed into mass loading (kg/m^2) by multiplying the thickness at each node by the bulk density of the deposit. Bulk density of fallout deposits was measured by weighting a known volume of actual deposit. Moreover, the bulk density of Plinian deposits was allowed to vary, depending on the variations of grain-size and components (Table 1). The result of these calculations was the construction of a set of maps of isomass on the ground for each eruption (100–400 kg/m^2). Figure 3 shows the total mass loading for the considered 24 tephra fallout deposits.

[13] The large number of measured stratigraphic sections (>100) and their evenly spaced distribution represents a homogeneous data set, with a comparable accuracy for all the eruptions, which allowed the definition of the field frequency. This relative frequency is calculated at each node of the grid as the ratio between the number of eruptions

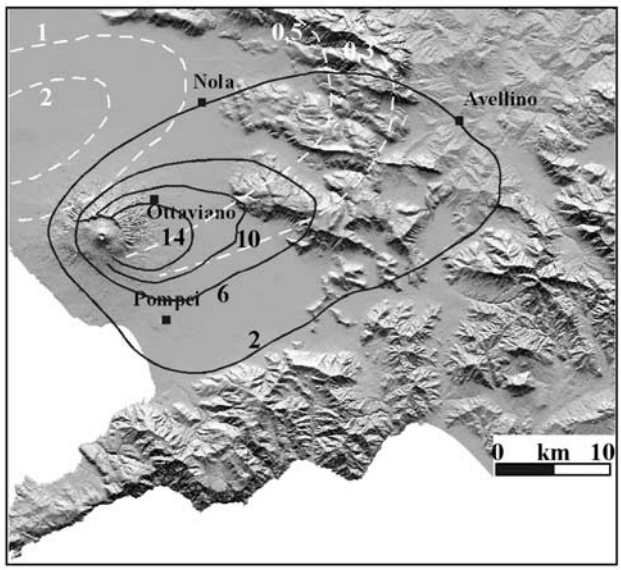

Figure 3. Total mass loading (ton/m^2) from fallout deposits of the last 18 ka Vesuvius (black lines) and Phlegrean Fields (white lines) volcanoes.

giving a mass loading greater than the chosen threshold and the total number of eruptions considered. From the same data set, relative frequency can also be assessed for a subset of data representing a given class of events (eruptions of similar magnitude eruptions in a certain time interval).

[14] Up to now, hazard maps for tephra fallout have generally been constructed based on thickness of the deposits of selected eruptions [*Booth*, 1979; *Crandell et al.*, 1984; *Blong*, 1984; *Baker*, 1985] or taking into account the statistics of wind direction [*Crandell and Mullineaux*, 1975; *Westercamp*, 1980; *McKee et al.*, 1985; *Miller*, 1989]. In contrast, the maps of mass loading give a more precise picture of the hazard. The possibility to consider a quite complete record of the natural variability of the past activity allows the discussion of data in terms of probability. Applying the maximum likelihood principle, the field frequency can be considered the proxy for the probability. Using actualism, the number of eruptive deposits per unit time at a given site is used as a proxy for probability of future eruptions of similar magnitude affecting that site.

[15] In Figure 4, field frequency of a mass loading greater than 200 kg/m^2 of tephra is shown as an example. This map represents a faithful picture of all the past events, and the size and shape of the curves are a function of the natural range of eruption magnitude and intensity shown by Vesuvius during the last 18,000 years. Similar maps, obtained for a subset of eruptions with VEI between 3 and 5 (in the range of MEE) and thresholds of 100, 200, 300, and 400 kg/m^2 are shown in Figure 5.

4.2. Probability of Tephra Fallout From Numerical Modeling of the MEE: Simulated Probability Method

[16] A 3-D model of pyroclastic particle fallout from a sustained eruption column [*Armienti et al.*, 1988] was tested and validated on the Plinian A.D. 79 Vesuvius eruption [*Macedonio et al.*, 1988]. In this paper, a 2-D simplified version of the model is used to obtain MEE-based hazard maps. The model is based on the solution of a 2-D transport equation for tephra particles, accounting for the advection of wind, the settling of particles and the atmospheric turbulent diffusion. Vertical diffusion and wind advection are neglected. As well, the model does not account for ballistic dispersal and the complex effects of clast dispersal near the volcano, so suffering an inherent bias in the calculation of proximal deposits, which was evidenced by *Bursik et al.* [1992]. Assuming a certain value of eddy diffusion coefficients and the vertical distribution of mass along the column [*Suzuki*, 1983; *Macedonio et al.*, 1990; *Barberi et al.*, 1990], the input data of the model are the total erupted mass, the wind velocity, the column height and the grain-size distribution of the eruptive mixture at the vent. Because of the simplifying assumption on the column features, the model is appropriate for the calculation of fall deposits at distances greater than the vertical spacing of the column discretization [*Macedonio et al.*, 1990]. The output of the model is a mass loading (in kg/m^2) distribution on the ground, from which the isomasses or isopachs of the simulated fallout deposit can be traced.

[17] To verify its applicability to eruptions smaller than Plinian, the model was initially tested by simulating the fallout of the sub-Plinian A.D. 1631 eruption. Although the fallout deposit suggests a clockwise rotation of wind with distance [*Rosi et al.*, 1993], an average wind direction was imposed on the basis of the tephra dispersal. Following *Carey and Sparks* [1986], a typical midlatitude wind velocity profile was assumed, linearly increasing with height up to a maximum at the tropopause, and with a stratospheric value equal to the 3/4 of the tropopause maximum. In the simulations, the less constrained parameters were allowed to vary: the tropopause height (from 11 to 13 km); the wind speed at the tropopause (considered of 20, 30, and 40 m/s); the column height (between 12 and 22 km, according to the results of *Rosi et al.* [1993]); the mass erupted for each particle size. An ''artificial'' deposit was calculated for each

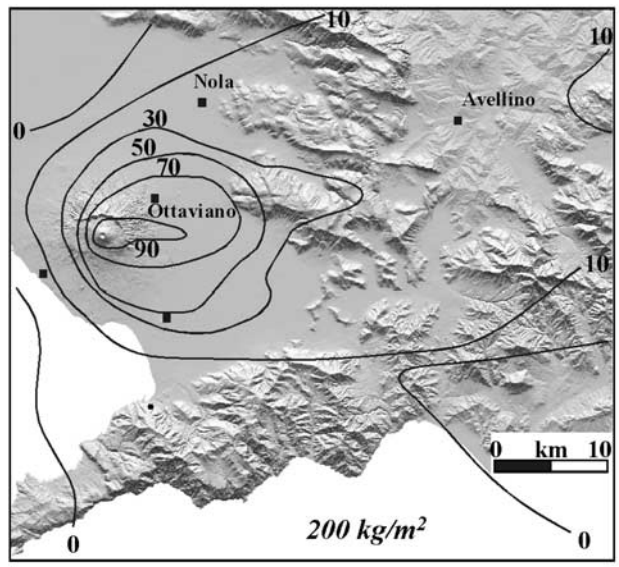

Figure 4. Frequency (%) of occurrence of tephra loading greater than 200 kg/m^2 from all the explosive events of the last 18 ka Vesuvius activity.

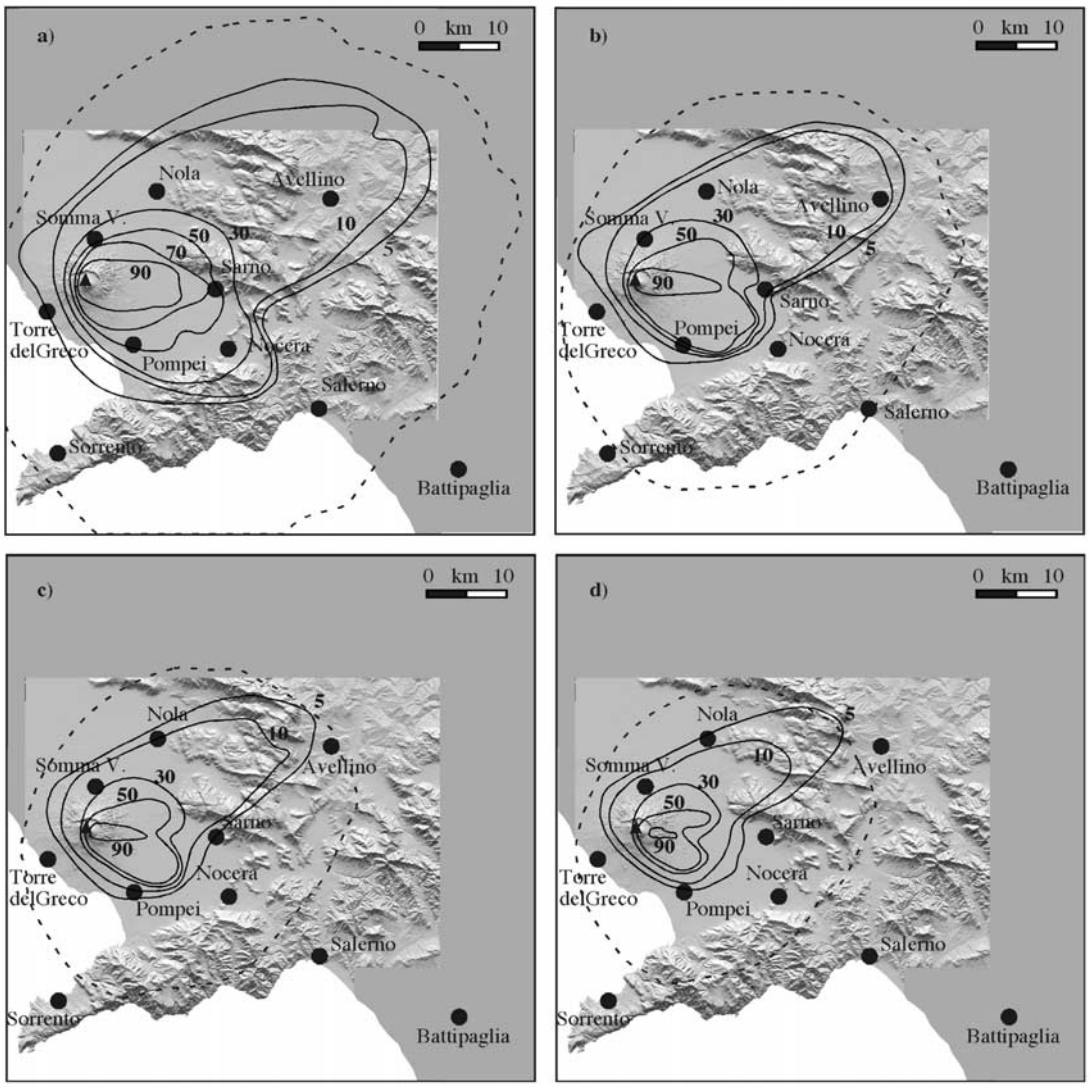

Figure 5. Frequency of occurrence (%) of tephra loading greater than (a) 100 kg/m^2, (b) 200 kg/m^2, (c) 300 kg/m^2, and (d) 400 kg/m^2 from the VEI 3/5 explosive events of the last 18 ka Vesuvius activity. For comparison, the 5% probability curve from numerical simulations is shown (dashed line).

different combination of these parameters. Each artificial deposit was then compared with the field data, and the least squares were calculated to select those cases that gave the best fit with the field data. Thus, the results of the least squares fit are sets of input parameters all representing equivalent choices of the values that best replicate the deposit of the A.D. 1631 eruption. In particular, the masses of each particle size, which give the best fit to the field data, define a grain-size population representative of the eruptive mixture at the vent (1631-type distribution of Figure 6). The best fitting artificial deposit is compared in Figure 7 with the field data, showing a generally satisfactory consistency. Main discrepancies occur for high (100 cm) thickness and are probably an inherent bias of the model, which does not account for ballistics and, generally, for the effects on clast dispersal in areas close to the vent.

[18] Once the model was validated, a parametric study was performed on the input data, in order to define the role of the main parameters (and of their uncertainties) in controlling the distribution of hazard probabilities. In order to simulate the MEE, the total grain-size population of the eruptive mixture and the column height have to be chosen. Two different particle populations of the eruptive mixture have been considered, to account for the generally different density and size distribution of the clasts of Plinian and sub-Plinian fall deposits: (1631-type and 79-type distributions of Figure 6). To account for the possible significant loss of fines from the column, a third particle population was created, by increasing up to 50% by weight the fine fraction in the 1631-type population (''1631 fines enriched'', Figure 6).

[19] As discussed above, a MEE with a maximum eruptible mass of 5×10^{11} kg can be inferred from the model of behavior accepted for the volcano. As the total mass erupted during the past events of similar size is not clearly related to the intensity of the eruption [*Andronico and Cioni*, 2002; *Arrighi et al.*, 2001] the column height for the MEE simulations was allowed to vary in a range between 12 and 22 km.

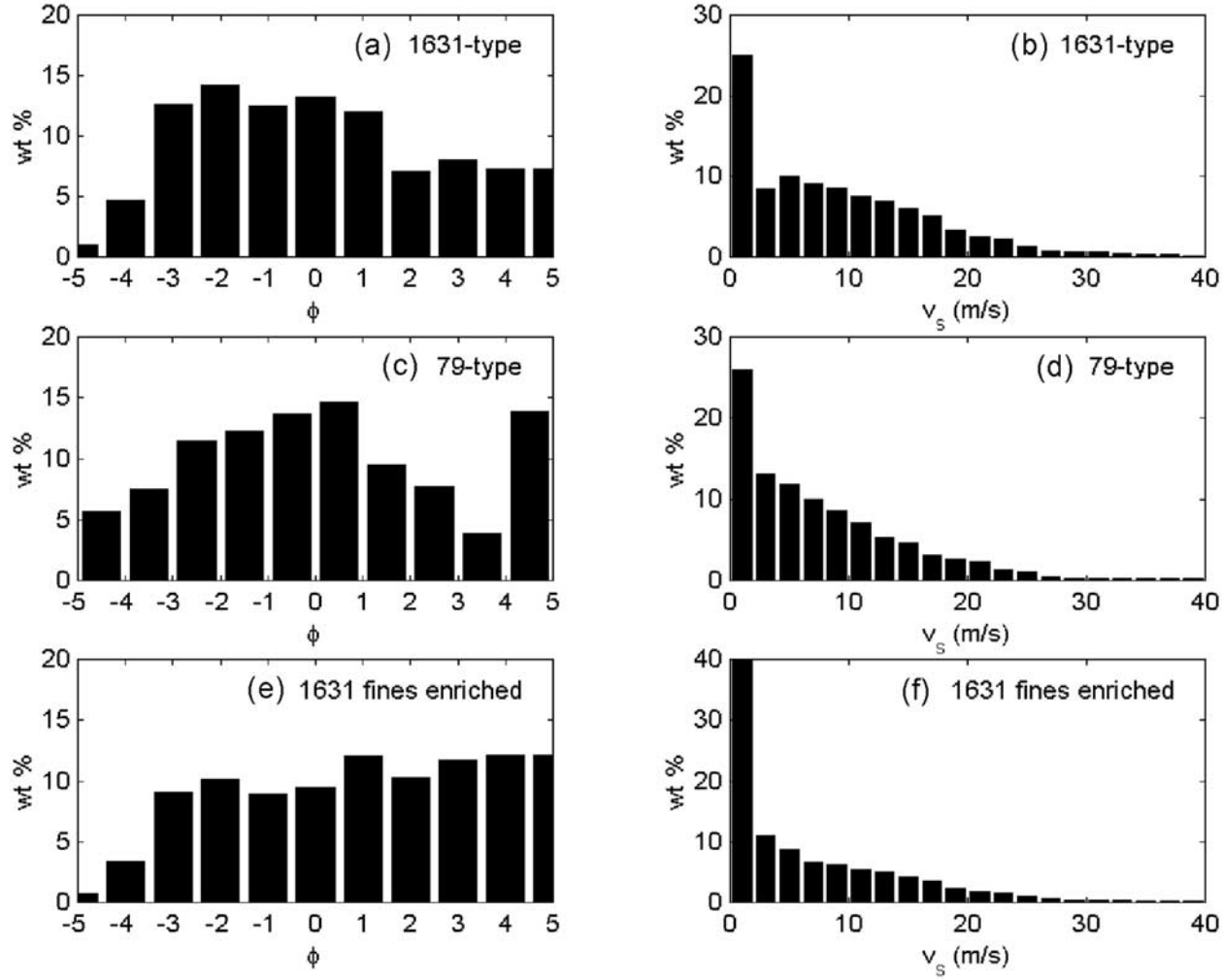

Figure 6. (a), (c), (e) Grain size and (b), (d), (f) settling velocity distributions used in the numerical modeling of the MEE.

[20] In order to account for the uncertainties in the input parameters, numerical simulations of the fallout deposit were reiterated for different wind fields (3125 cases), considering three eruptive masses (1/2 of the MEE mass, the MEE mass and 3/2 of the MEE mass), six column heights (12, 14, 16, 18, 20, and 22 km), and three particle populations (79, 1631, and 1631 fines enriched), producing 54 different sets. The mass loading of the deposit was computed for a total area of 200 × 200 km, on a regular grid with 1 km spacing. The differences in input data between our modeling and that of *Barberi et al.* [1990] are summarized in Table 2.

[21] The 3125 wind profiles result from data collected at the Brindisi Meteo STAT over 14 years of observation, thus representing the statistical winds distribution in the area which is potentially involved in tephra dispersal. As in the hazard assessment from field data, mass loadings of 100, 200, 300 and 400 kg/m^2 were considered.

[22] The probability of exceeding a threshold, given as the percent of simulations producing a deposit heavier than the chosen threshold, was calculated at each node of the grid for each set of simulations. The results of simulations using different grain-size distribution, column height and total

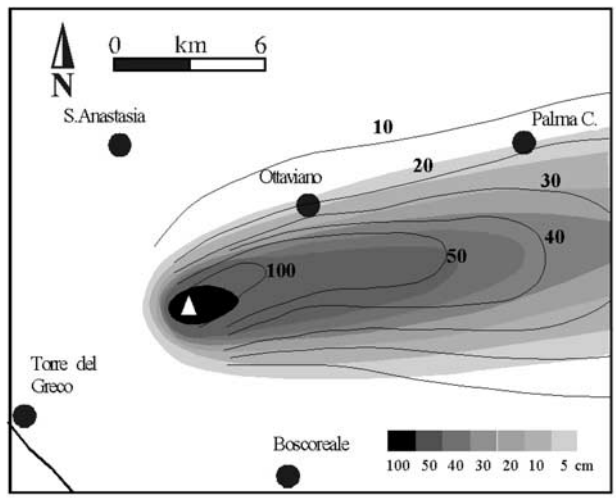

Figure 7. Comparison between the A.D. 1631 isopach map [*Rosi et al.*, 1993] and results from the numerical simulation of the same eruption (gray scale). Input data for simulations are column height 22 km, stratospheric wind 30 m/s, and maximum wind 40 m/s.

Table 2. Main Differences Between Data Used in This Paper and Those Used by *Barberi et al.* [1990]

Data	*Barberi et al.* [1990]	This Paper
Erupted mass, $\times 10^{11}$ kg	2	5
Column height, km	13	12–22
Particle population	A.D. 79-type	A.D. 1631-type A.D. 79-type A.D. 1631 "fine enriched"

mass show a different sensitivity of the model to each of these variables (Figure 8).

[23] Erupted mass is the most important parameter in changing tephra dispersal, greatly enlarging isoprobability areas when varied in a range consistent with the uncertainty in the estimation (evaluated at ±50%) for a fixed mass, tephra dispersal results are more influenced by variations of column height than grain-size distributions of the eruptive mixture (Figures 8a, 8b, and 8c).

[24] Keeping in mind the high sensitivity of the model to mass variations, "final" hazard maps from numerical modeling were traced for the MEE mass (5×10^{11} kg), the 1631 pyroclastic particle distribution and averaging the results for column heights between 12 and 22 km (Figure 9).

[25] The average wind distribution is almost isotropic at heights lower than 8 km and eastward for greater heights. A corollary of this situation is that lower eruption columns produce a more symmetric probability distribution and greater hazard in the westward direction than higher columns.

5. Discussion

[26] The two approaches both suffer limitations: geological data can suffer from incomplete preservation of the stratigraphic record or of low eruptive frequency, leading to a statistically unsatisfactory record. Furthermore, the use of geological data is appropriate only when they encompass to

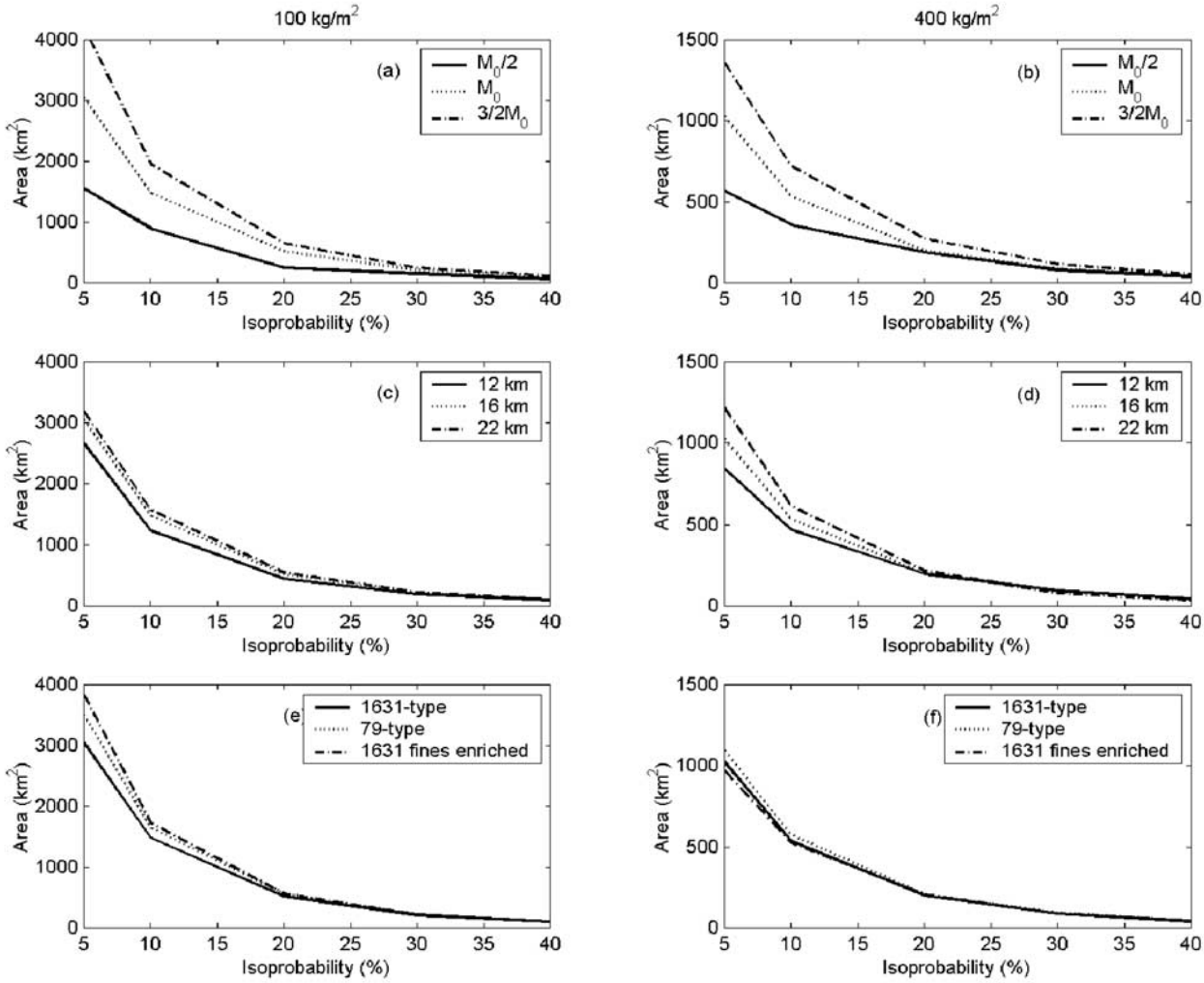

Figure 8. Sensitivity of the numerical model to the input parameters. Comparison between areas enclosed by isoprobability contours for the 100 and 400 kg/m^2 thresholds: (a), (b) 1631-type grain size, column height of 16 km, different erupted masses ($M_0/2$, M_0, $3/2M_0$); (c), (d) 1631-type grain-size, column heights of 12, 16 and 22 km, M_0 erupted mass; (e), (f) different grain sizes (1631-type, 79-type, "1631 fines enriched"), column height of 16 km, M_0 erupted mass.

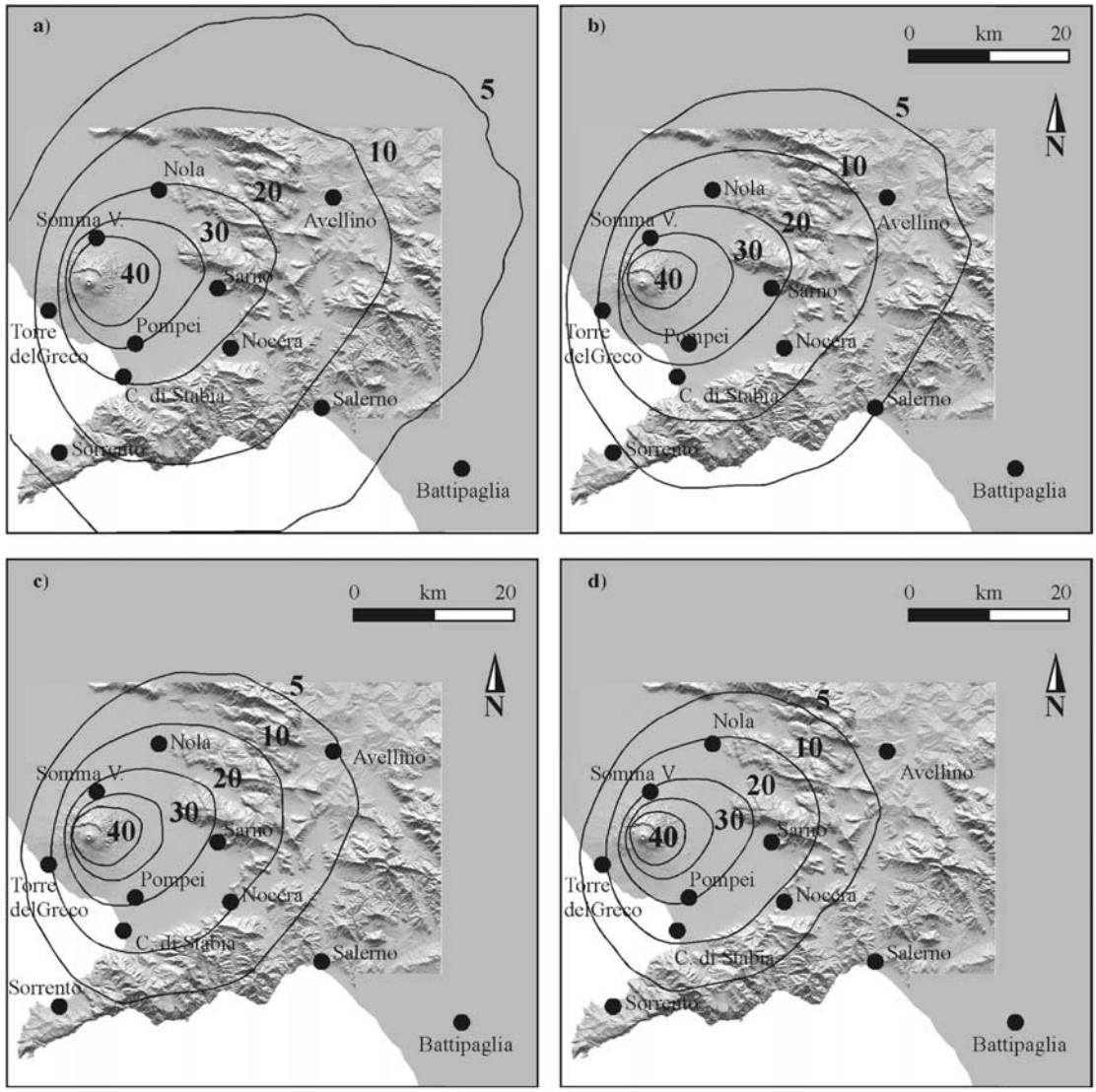

Figure 9. Probability of occurrence of a mass loading greater than (a) 100 kg/m^2, (b) 200 kg/m^2, (c) 300 kg/m^2, and (d) 400 kg/m^2 from numerical simulation.

a period of the volcano history in which no primary changes occurred in its mode of operation.

[27] Data derived from numerical simulations generally have a weak point in the simplifying assumptions of their equations and in neglecting important factors such as enhanced proximal deposition (by ballistic dispersal and sedimentation from inside the column edges) and ash aggregation. Proximal sedimentation remains a main flaw in the model, and it is suggested in the following that this can be circumvented by using data derived from the field frequency method. On the other hand, due to the quite coarse grain size distribution of the erupting mixture used in the modeling (Figure 8), ash aggregation becomes important only in the fine-grained, thin, distal deposits, corresponding to mass loading values well below the selected threshold. Furthermore, modeling of future eruptions is also strongly dependent on the expected magnitude and intensity of the MEE, which derives from the model of operation accepted for the volcano.

[28] When comparing isoprobability maps (Figures 5 and 9), major differences emerge in the most proximal areas (<10 km from the vent) where the geological data have the maximum statistical reliability (thanks to the higher density of measured sections) while the numerical simulation suffer major uncertainties due to the neglecting of ballistic deposition and the oversimplified assumption on mass distribution along the column [*Suzuki*, 1983]. The discrepancy amounts to at least a factor 2 in the >30% probability values (Figure 10a), suggesting that for such high probabilities, geological data give a more accurate picture of the expected hazard. On the other hand, the wider areas subjected to hazard probability <30% shown by the maps obtained from the numerical simulations reflect the larger wind statistics than the past events, which sampled only a small subset of the whole population of wind fields.

[29] The two methods are therefore complementary and the most reliable hazard maps result from their combination. The 200 kg/m^2 example is shown in Figure 10b, where the

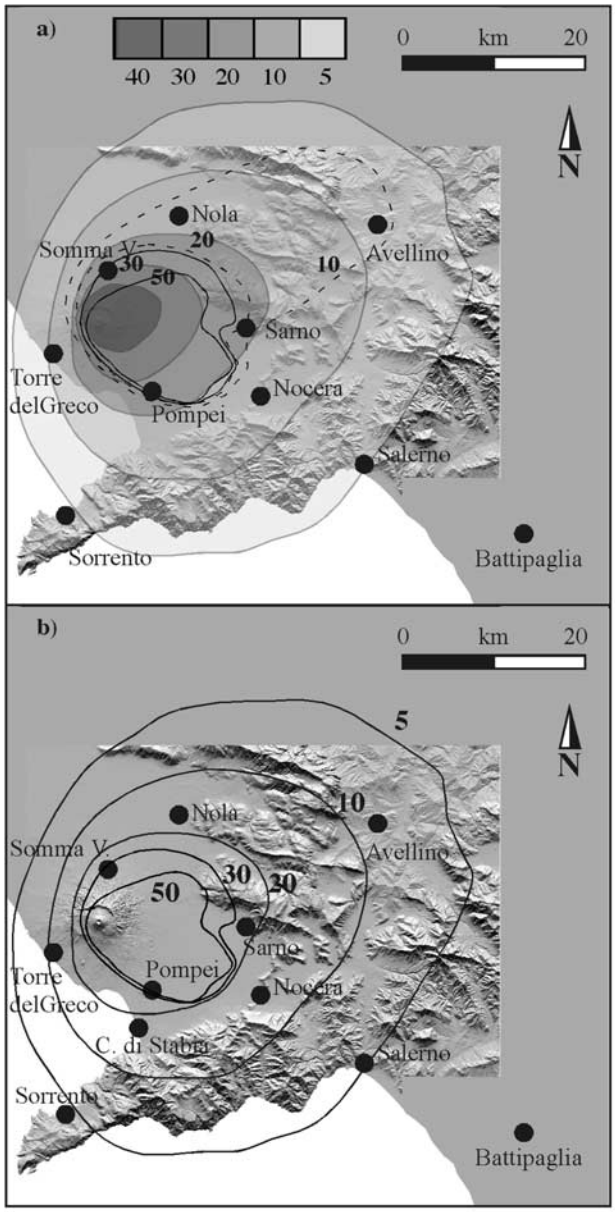

Figure 10. (a) Comparison of field-based and numerical simulation maps for tephra loading >200 kg/m^2 and (b) final hazard map for tephra loading >200 kg/m^2, as results from the merging of field studies and numerical simulations.

<30% probability values come from the geological data and the >30% from the numerical simulations.

6. Conclusions

[30] Two methods have been discussed for assessing tephra fallout hazard through the estimation of the probability of mass loading greater than given thresholds: (1) field frequency based on field data and (2) simulated probability obtained by reiterating simulations of the MEE using actual wind statistics.

[31] Vesuvius is suitable for the application of both methods because of (1) the extensive knowledge of its eruptive history and fallout deposits distribution and features, allowing the reconstruction of "probability" geological maps, which are not common in hazard literature; and (2) the reliability of the general operational model of the volcano and hence of the chosen MEE.

[32] A further complication to fallout hazard assessment in the Vesuvian area, is the proximity of the Phlegrean Fields caldera, whose products are mainly dispersed in an area interfering with the Vesuvius deposits (Figure 3). It has to be strongly recommended that hazard assessment in these two areas be done with comparable methods, in order to allow the merging of the results in a volcanic hazard map for the whole Campanian Plain.

[33] **Acknowledgments.** We acknowledge the Senior Editor F. Albarede, C. Bonadonna, and the other JGR reviewers for their helpful comments. The research was done with funding of the Gruppo Nazionale di Vulcanologia.

References

Andronico, D., La stratigrafia dei prodotti dell'eruzione di Lagno Amendolare Campi Flegrei, Napoli, *Atti Soc. Toscana. Sci. Nat. Pisa Mem., Ser. A*, *104*, 165–178, 1997.

Andronico, D., and R. Cioni, Contrasting styles of Mount Vesuvius activity in the period between the Avellino and Pompeii Plinian eruptions, and some implications for assessment of future hazards, *Bull. Volcanol.*, *64*, 372–391, 2002.

Andronico, D., G. Calderoni, R. Cioni, A. Sbrana, R. Sulpizio, and R. Santacroce, Geological map of Somma-Vesuvius volcano, *Period. Mineral.*, *64*(1–2), 77–78, 1995.

Armienti, P., G. Macedonio, and M. T. Pareschi, A numerical model for the simulation of tephra transport and deposition: Applications to May 18, 1980, Mount St. Helens eruption, *J. Geophys. Res.*, *93*(B6), 6463–6476, 1988.

Arrighi, S., C. Principe, and M. Rosi, Violent Strombolian and subplinian eruptions at Vesuvius during post-1631 activity, *Bull. Volcanol.*, *63*, 126–150, 2001.

Baker, P. E., Volcanic hazard on St. Kitts and Montserrat, West Indies, *J. Geol. Soc. London*, *142*, 279–295, 1985.

Barberi, F., G. Macedonio, M. T. Pareschi, and R. Santacroce, Mapping the tephra fallout risk: An example from Vesuvius (Italy), *Nature*, *344*, 142–144, 1990.

Bertagnini, A., P. Landi, M. Rosi, and A. Vigliargio, The Pomici di Base Plinian eruption of Somma-Vesuvius, *J. Volcanol. Geotherm. Res.*, *83*, 219–239, 1998.

Blong, R. J., Volcanic Hazards, *A Sourcebook on the Effects of Eruptions*, Academic, San Diego, Calif., 1984.

Booth, B., Assessing volcanic risk, *J. Geol. Soc. London*, *136*, 331–340, 1979.

Bursik, M. I., R. S. J. Sparks, J. S. Gilbert, and S. N. Carey, Sedimentation of tephra by volcanic plumes, I, Theory and its comparison with a study of the Fogo: A Plinian deposit, Sao Miguel (Azores), *Bull. Volcanol.*, *54*, 329–344, 1992.

Carey, S., and R. S. J. Sparks, Quantitative models of the fallout and dispersal of tephra from volcanic eruption columns, *Bull. Volcanol.*, *48*, 109–125, 1986.

Cherubini, A., S. M. Petrazzuoli, and G. Zuccaro, Vulnerabilità sismica dell'area Vesuviana, publication, Gruppo Naz. per la Difesa dai Terremoti, Rome, 2001.

Cioni, R., L. Civetta, P. Marianelli, N. Metrich, R. Santacroce, and A. Sbrana, Compositional layering and syn-eruptive mixing of a periodically refilled shallow magma chamber: The A.D. 79 Plinian eruption of Vesuvius, *J. Petrol.*, *36*(3), 739–776, 1995.

Cioni, R., P. Marianelli, and R. Santacroce, Thermal and compositional evolution of the shallow magma chambers of Vesuvius: Evidence from pyroxene phenocrysts and melt inclusions, *J. Geophys. Res.*, *103*(B8), 18,277–18,294, 1998.

Cioni, R., R. Santacroce, and A. Sbrana, Pyroclastic deposits as a guide for reconstructing the multi-stage evolution of the Somma-Vesuvius Caldera, *Bull. Volcanol.*, *60*, 207–222, 1999.

Cioni, R., S. Levi, and R. Sulpizio, Apulian Bronze Age pottery as a long-distance indicator of the Avellino Pumice eruption (Vesuvius, Italy), in *The Archaeology of Geological Catastrophes*, edited by W. G. McGuire et al., *Geol. Soc. Spec. Publ., 171*, 159–177, 2000.

Civetta, L., and R. Santacroce, Steady-state magma supply in the last 3,400 years of Vesuvius activity?, *Acta Vulcanol.*, *2*, 147–160, 1992.

Cortini, M., and R. Scandone, The feeding system of Vesuvius between 1754 and 1944, *J. Volcanol. Geotherm. Res.*, *12*, 393–400, 1982.

Crandell, D. R., and D. R. Mullineaux, Technique and rationale of volcanic hazards appraisals in the Cascade Range, northwestern United States, *Environ. Geol.*, *1*, 23–32, 1975.

Crandell, D. R., B. Booth, K. Kazumadinata, D. Shimuzuru, G. P. L. Walker, and D. Westercamp, *Natural Hazards*, vol. 4, *Source-Book for Volcanic-Hazards Zonation*, 97 pp., UNESCO, Geneva, 1984.

de Vita, S., et al., The Agnano-Monte Spina eruption (4,100 years BP) in the restless Campi Flegrei Caldera (Italy), *J. Volcanol. Geotherm. Res.*, *91*, 269–301, 1999.

Di Girolamo, P., M. R. Ghiara, L. Lirer, R. Munno, G. Rolandi, and D. Stanzione, Vulcanologia e petrologia dei Campi Flegrei, *Boll. Soc. Geol. It.*, *103*(2), 349–413, 1984.

Macedonio, G., M. T. Pareschi, and R. Santacroce, A numerical simulation of the Plinian fall phase of the 79 A.D. eruption of Vesuvius, *J. Geophys. Res.*, *93*(B12), 14,817–14,827, 1988.

Macedonio, G., M. T. Pareschi, and R. Santacroce, Renewal of volcanic activity at Vesuvius: Tephra fallout, *J. Volcanol. Geotherm. Res.*, *40*, 327–342, 1990.

Marianelli, P., N. Metrich, R. Santacroce, and A. Sbrana, Mafic magma batches at Vesuvius: A glass inclusion approach to the modalities of feeding stratovolcanoes, *Contrib. Mineral. Petrol.*, *120*, 159–169, 1995.

McKee, C. O., R. W. Johnson, P. L. Lowenstein, S. J. Riley, R. J. Blong, P. De Saint'Ours, and B. Talai, Rabaul caldera, Papua New Guinea: Volcanic hazards, surveillance, and eruption contingency planning, *J. Volcanol. Geotherm. Res.*, *23*, 195–237, 1985.

Miller, C. D., Potential hazards from future volcanic eruptions in California, *U.S. Geol. Surv. Bull., 1847*, 17 pp., 1989.

Newall, C. G., and S. Self, The volcanic explosivity index (VEI): An estimate of explosive magnitude for historical volcanism, *J. Geophys. Res.*, *87*, 1231–1238, 1982.

Orsi, G., M. D'Antonio, S. de Vita, and G. Gallo, The Neapolitan Yellow Tuff, a large-magnitude trachytic phreatoplinian eruption: Eruptive dynamics, magma withdrawal and caldera collapse, *J. Volcanol. Geotherm. Res.*, *53*, 275–287, 1992.

Pyle, D. M., The thickness, volume and grainsize of tephra fall deposits, *Bull. Volcanol.*, *51*, 1–15, 1989.

Rolandi, G., A. M. Barrella, and A. Borrelli, The 1631 eruption of Vesuvius, *J. Volcanol. Geotherm. Res.*, *58*, 183–201, 1993.

Rosi, M., and R. Santacroce, The A.D. 472 "Pollena" eruption: volcanological and petrological data from this poorly known Plinian-type event at Vesuvius, *J. Volcanol. Geotherm. Res.*, *17*, 249–271, 1983.

Rosi, M., C. Principe, and R. Vecci, The 1631 Vesuvian eruption: A reconstruction based on historical and stratigraphical data, *J. Volcanol. Geotherm. Res.*, *58*, 151–182, 1993.

Santacroce, R., (Ed.), *Somma-Vesuvius, Monografia*, vol. 114(8), 230 pp., Quad. de La Ric. Sci., CNR, Rome, 1987.

Santacroce, R., A. Bertagnini, L. Civetta, P. Landi, and A. Sbrana, Eruptive dynamics and petrogenetic processes in a very shallow magma reservoir: The 1906 eruption of Vesuvius, *J. Petrol.*, *34*, 383–425, 1993.

Santacroce, R., R. Cioni, L. Civetta, P. Marianelli, N. Metrich, and A. Sbrana, How Vesuvius works, in *Atti Convegno*, vol. 112, pp. 185–196, Accad. Naz. dei Lincei, Rome, 1994.

Suzuki, T., A theoretical model for dispersion of tephra, in *Arc Volcanism: Physics and Tectonics*, edited by D. Shimozuru and I. Yokoyama, pp. 93–113, Terra Sci., Tokyo, 1983.

Westercamp, D., Une methode d'evaluation et de zonation des risques volcaniques a la Soufriere de Guadeloupe, Antilles Francaises, *Bull. Volcanol.*, *43*, 431–452, 1980.

D. Andronico, INGV- Catania, via Montirossi 12, 95030, Nicolosi Catania, Italy.

R. Cioni, Dipartimento di Scienze della Terra, Università degli Studi di Cagliari, via Trentino 51, 09127, Cagliari, Italy. (rcioni@unica.it)

A. Longo, R. Santacroce, A. Sbrana, and R. Sulpizio, Dipartimento di Scienze della Terra, Università degli Studi di Pisa, via S. Maria 53, 56126, Pisa, Italy. (longo@dst.unipi.it; santacroce@dst.unipi.it; sbrana@dst.unipi.it; sulpizio@dst.unipi.it)

G. Macedonio, INGV-Osservatorio Vesuviano, via Diocleziano 328, 80124, Napoli, Italy. (macedon@ov.ingv.unina.it)